Cardiac Sodium Channel Markov Model with Temperature Dependence and Recovery from Inactivation

Lisa A. Irvine, M. Saleet Jafri, and Raimond L. Winslow
Department of Biomedical Engineering, Center for Computational Medicine and Biology, The Johns Hopkins University School of Medicine, Baltimore, Maryland 21205 USA

ABSTRACT A Markov model of the cardiac sodium channel is presented. The model is similar to the CA1 hippocampal neuron sodium channel model developed by Kuo and Bean (1994. *Neuron.* 12:819–829) with the following modifications: 1) an additional open state is added; 2) open-inactivated transitions are made voltage-dependent; and 3) channel rate constants are exponential functions of enthalpy, entropy, and voltage and have explicit temperature dependence. Model parameters are determined using a simulated annealing algorithm to minimize the error between model responses and various experimental data sets. The model reproduces a wide range of experimental data including ionic currents, gating currents, tail currents, steady-state inactivation, recovery from inactivation, and open time distributions over a temperature range of 10°C to 25°C. The model also predicts measures of single channel activity such as first latency, probability of a null sweep, and probability of reopening.

INTRODUCTION

For many years Hodgkin-Huxley models (Hodgkin and Huxley, 1952a, b) have been the standard for describing ionic current kinetics. However, with the development of better recording techniques, new data have shown that these models have significant limitations. First, many single channel behaviors such as mean open time and first latency cannot be described using traditional Hodgkin-Huxley models. These behaviors can be estimated by expanding the Hodgkin-Huxley models to have multiple resting and inactivated states, but it is controversial as to how well these expanded models can predict single channel experimental data (Horn and Vandenberg, 1984; Chay, 1991). Second, while a Hodgkin-Huxley model can reproduce ionic currents, it does not necessarily correctly reproduce the underlying single channel kinetics. For example, Aldrich and co-workers found that for neuroblastoma sodium channels, activation has very slow components, while inactivation is fast (Aldrich et al., 1983). This finding contradicts Hodgkin's and Huxley's assumption that activation is rapid and inactivation is slow (Hodgkin and Huxley, 1952a, b). Even though Hodgkin-Huxley models can reproduce this current, they do not correctly reproduce the underlying channel kinetics. Although single channel recordings of cardiac sodium channels indicate that activation is rapid relative to inactivation (Yue et al., 1989), it is questionable whether Hodgkin-Huxley models are sufficient for reproducing behaviors that may be critically state-dependent, such as how ionic channels interact with drugs and toxins (Irvine and Winslow, 1996; Liu and Rasmusson, 1997). In addition, since much more is now known about the structure of the sodium channel (Noda et al., 1984, 1986; Guy, 1988), it is desirable to incorporate this information into a description of channel function. Thus, future channel models should be biophysically detailed kinetic models, consistent with current generalizations of channel structure, capable of reproducing single channel behavior.

For the cardiac sodium channel, models that describe channel gating as a Markov process (Benndorf, 1988; Berman et al., 1989; Scanley et al., 1990) are a step in this direction. Existing models for the cardiac sodium channel are, however, incomplete in that they describe only certain features of channel behavior. Specifically, each of these models lacks rate constants with explicit voltage and temperature dependence. In addition, these models treat inactivation as an absorbing state, so that once a channel inactivates, there is no pathway by which it can recover. Thus, they can only be used to simulate certain channel behaviors in response to a single voltage clamp stimulus. They do not reproduce channel activity to the same extent as Hodgkin-Huxley models and therefore have not been as widely used.

More comprehensive Markov models exist for sodium channels of the squid giant axon (Patlak, 1991; Vandenberg and Bezanilla, 1991). Vandenberg and Bezanilla and Patlak have been able to develop these models by using a wide variety of both whole cell and single channel data simultaneously. Unfortunately, because of the many differences in channel kinetics between cardiac and neuronal tissue (Kirsch and Brown, 1989; Kuo and Bean, 1994; Hanck and Sheets, 1995; Fozzard and Hanck, 1996), these models cannot be used directly to model cardiac sodium channels. Nevertheless, the neuronal models and the techniques used to develop them are a starting point from which to develop a more complete model of the cardiac sodium channel.

Although Markov models exist from which cardiac sodium channel Markov models can be developed for a single

Received for publication 12 June 1998 and in final form 6 January 1999.
Address reprint requests to Raimond L. Winslow, The Johns Hopkins University School of Medicine, Department of Biomedical Engineering, 411 Traylor Building, 720 Rutland Avenue, Baltimore, MD 21205. Tel.: 410-502-5090; Fax: 410-614-0166; E-mail: rwinslow@bme.jhu.edu.

0006-3495/99/04/1868/18 $2.00

temperature, no models exist that can reproduce ensemble-average and single channel behaviors for a range of temperatures. The models of Vandenberg and Patlak have a temperature-dependent rate constant coefficient and a temperature-dependent voltage term (Patlak, 1991; Vandenberg and Bezanilla, 1991). Changing the temperature in these terms, however, does not yield the correct channel activity at multiple temperatures. Each term in the model's rate constants needs to have its own temperature dependence or its own Q_{10} factor (Kohlhardt, 1990). Temperature-dependent closed-closed and closed-open transitions have been incorporated into a partial model of neuronal sodium channels by formulating the rate constants as exponential functions of enthalpy and entropy (Correa et al., 1992). The same rate constant formulation can be used in a model of cardiac sodium channels to reproduce ensemble-average and single channel behaviors for a range of temperatures.

The goal of this study is to use neuronal models as a framework for developing a Markov model of the cardiac sodium channel. The model should exhibit correct macroscopic and single channel behavior, including recovery from inactivation, for a voltage range of −150 mV to 20 mV and a temperature range of 10°C to 25°C. Such a model would improve on existing Hodgkin-Huxley and Markov models significantly and may yield more insight into the molecular basis of channel function. In addition, such a model could be used as the basis for studies of antiarrhythmic drug action.

MODEL

The cardiac sodium channel Markov model is patterned after that by Kuo and Bean for sodium channels in CA1 hippocampal neurons (Kuo and Bean, 1994). This model is chosen as a starting point because it is consistent with current generalizations of channel structure, but uses symmetry and cooperative movement of the voltage sensors to reduce the number of free parameters. As shown in Fig. 1, the channel can occupy any of 13 states. The top row of states corresponds to zero to four voltage sensors being activated (C_0 through C_4) plus an additional conformational change required for opening ($C_4 \rightarrow O_1$ and $C_4 \rightarrow O_2$). The bottom row of states corresponds to the inactivation particle blocking the pore at each position of the voltage sensors. As in Kuo and Bean's model, the affinity of the inactivation particle binding site is hypothesized to increase by a scaling factor (a) as the channel activates and to decrease by the same factor as the channel deactivates. Closed-closed and closed-open transitions (horizontal transitions) are voltage-dependent, and closed-inactivated transitions (vertical transitions) are voltage-independent (Kuo and Bean, 1994).

In order to represent the cardiac sodium channel more accurately, two modifications are made to the Kuo and Bean model. The first modification is that an additional open state (O_2), with the same conductance as the first, is added. Transitions between the two open states are voltage-independent. The addition of a second open state provides another pathway by which the channel can open ($C_4 \rightarrow O_2$) and improves the fit to the decay of the ionic currents. Two arguments can be made for the existence of more than one open state. First, although single channel open time distributions are generally well fit by a single exponential (Patlak and Oritz, 1985; Berman et al., 1989; Scanley et al., 1990), they can also be fit well by multiple exponentials, particularly in the presence of toxins (Kunze et al., 1985; Nagy, 1987; Schreibmayer and Jeglitsch, 1992; Correa and Bezanilla, 1994). Second, sodium channels from many tissues, including cardiac tissue, produce tail currents with two exponential components (Goldman and Hahin, 1978; Dubois and Schneider, 1982; Hanck and Sheets, 1995; Elinder and Arhem, 1997). Erlinder and Arhem suggest that, in the absence of a two-step deactivation, in which the first transition is a fast equilibrium and the second is slow, this biexponential decay can only be produced by two open states connected by different pathways to a common closed state (Elinder and Arhem, 1997).

The second modification of the Kuo and Bean model is that open-inactivated transitions are made voltage-dependent. The change in the open-inactivated rate constants is supported by Yue, Lawrence, and colleagues' finding that a voltage-dependent open-to-inactivated transition is necessary to produce the correct voltage dependence of channel reopenings and mean open times (Yue et al., 1989; Lawrence et al., 1991). It is also supported by Sheets' and Hanck's measurement of a significant component of gating current due to this transition (Sheets and Hanck, 1995).

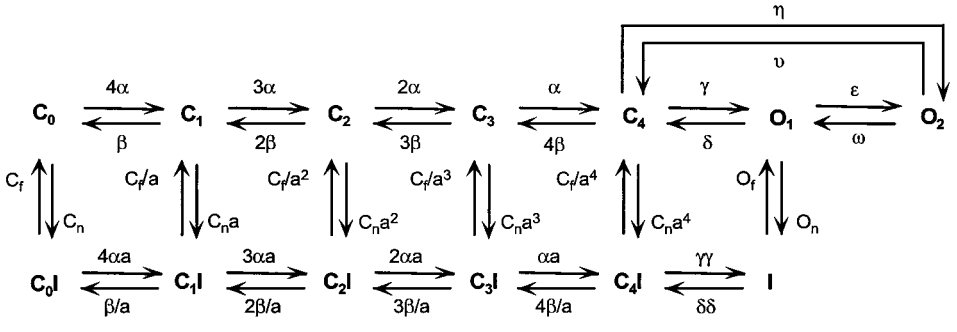

FIGURE 1 State diagram for the cardiac sodium channel Markov model. C_0–C_4 are closed states, O_1 and O_2 are open states, C_0I–C_4I are closed-inactivated states, and I is the inactivated state. All rate constants are voltage- and temperature-dependent except for those governing transitions between closed and closed-inactivated states, which are only temperature-dependent.

Rate constants are of the form from Eyring rate theory (Hille, 1992)

$$\lambda = \frac{kT}{h}\exp\left(\frac{-\Delta H_\lambda}{RT} + \frac{\Delta S_\lambda}{R} + \frac{z_\lambda F V}{RT}\right) \quad (1)$$

where k is the Boltzmann constant, T is the absolute temperature, h is the Planck constant, R is the gas constant, F is Faraday's constant, ΔH_λ is the change in enthalpy, ΔS_λ is the change in entropy, z_λ is the effective valence (i.e., the charge moved times the fractional distance the charge is moved through the membrane), and V is the membrane potential in volts. By convention, along the top row, all transitions toward an open state have positive valences because they are favored by depolarization, while those away from an open state have negative valences because they are favored by repolarization. The same convention is used along the bottom row; transitions toward the inactivated state have positive valences, while those away from the inactivated state have negative valences.

There are several loops in the model that must satisfy microscopic reversibility. Microscopic reversibility is derived from the law of conservation of energy and states that the product of rate constants when traversing a loop clockwise must be equal to the product when traversing the same loop counterclockwise (Hille, 1992). For the closed-closed-inactivated loops, satisfying microscopic reversibility requires that the transitions among the closed-inactivated states be scaled by a, the same factor used to scale the transitions between rows. Microscopic reversibility is preserved around the closed-open-inactivated loop by isolating the ΔH, ΔS, and z terms in the product and satisfying each term separately using the following equations:

$$\Delta H_{\gamma\gamma} = \Delta H_\gamma + \Delta H_{on} + \Delta H_{\delta\delta} + \Delta H_{cf} + 8\,RT\ln a - \Delta H_\delta - \Delta H_{cn} - \Delta H_{of} \quad (2)$$

$$\Delta S_{\gamma\gamma} = \Delta S_\gamma + \Delta S_{on} + \Delta S_{\delta\delta} + \Delta S_{cf} - \Delta S_\delta - \Delta S_{cn} - \Delta S_{of} \quad (3)$$

$$z_{\gamma\gamma} = z_\gamma + z_{on} + z_\delta + z_{of} - z_{\delta\delta} \quad (4)$$

Similarly, microscopic reversibility is preserved around the closed-open-open loop using the following equations for ΔH_η, ΔS_η, and z_η:

$$\Delta H_\eta = \Delta H_\gamma + \Delta H_\varepsilon + \Delta H_\nu - \Delta H_\delta - \Delta H_\omega \quad (5)$$

$$\Delta S_\eta = \Delta S_\gamma + \Delta S_\varepsilon + \Delta S_\nu - \Delta S_\delta - \Delta S_\omega \quad (6)$$

$$z_\eta = z_\gamma + z_\delta - z_\nu. \quad (7)$$

METHODS

Model development

The probability of occupying any particular channel state is described mathematically by a set of ordinary differential equations, written in matrix notation as

$$\frac{\partial \mathbf{P}(t)}{\partial t} = \mathbf{W}\mathbf{P}(t), \quad (8)$$

where $\mathbf{P}(t)$ is a vector describing the probabilities of occupying each state and $\mathbf{W}$ is the transition matrix. In general, $\mathbf{W}$ will be a function of voltage and thus time. For voltage-clamped conditions, however, $\mathbf{W}$ is time-independent; thus Eq. 8 has the analytic solution

$$\mathbf{P}(t) = \exp(\mathbf{W}t)\mathbf{P}(0). \quad (9)$$

Equation 9 is solved on a Silicon Graphics computer using linear algebra subroutines from the Silicon Graphics mathematics library (complib.sgimath).

Parameters of the model are determined using a simulated annealing algorithm (Corana et al., 1987). This algorithm minimizes the cost function, which is the weighted sum of the least-squared errors between model responses and experimental data, by randomly searching the parameter space and incrementally decreasing the search radius. Whereas many minimization algorithms accept only downhill moves and tend to converge on local minima, the simulated annealing algorithm accepts uphill moves as well, and thus is more likely to find the global minimum. Uphill moves are accepted based on the Metropolis criterion, a probabilistic function determined from the difference between the new and old errors and the annealing temperature. The annealing temperature controls the rate of convergence by influencing what uphill moves are accepted and by limiting the search radius. In order to reach a minimum, the annealing temperature is decreased by 5% per 50 N function evaluations, where N is the number of parameters to be determined, as the algorithm converges on a solution. The algorithm is terminated when there is no more than 0.1% change in error since the last temperature reduction.

In order to limit the number of free parameters to be determined during each minimization, the fitting procedure is done in parts. First, the enthalpy and entropy terms are collapsed into a single Gibbs free energy term and the Gibbs free energies and effective valences are determined for a temperature of 13°C. Then, holding the effective valences constant, the enthalpy and entropy terms are determined. The entropy terms are written in terms of the enthalpy and the Gibbs free energy (ΔG):

$$\frac{\Delta S_\lambda}{R} = \frac{\Delta H_\lambda - \Delta G_\lambda}{RT} \quad (10)$$

where T is the temperature, 286 K. Since the Gibbs free energies and valences are known from the previous minimization, substitution of Eq. 10 into Eq. 1 leaves only the enthalpies to be determined. The enthalpies are determined by fitting experimental data at 21°C using the simulated annealing algorithm.

As shown by Vandenberg and Bezanilla (1991) and Patlak (1991) in developing models of sodium channels in squid giant axon, a variety of experimental data sets are needed to fully determine the model parameters. In this study, the experimental data for 13°C include ionic currents (provided by Hanck and Sheets, similar to Sheets et al., 1996), gating charge accumulation (Hanck and Sheets as above), the steady-state inactivation curve (Hanck and Sheets as above), the rate of tail current relaxation (Hanck and Sheets, 1995), the time course of recovery from inactivation (Sakakibara et al., 1993), and single channel open times (Sheets and Hanck, 1995). The majority of data are taken from hH1 sodium channels or, where these data are unavailable, from canine sodium channels. Recovery data at 13°C are unavailable, so data at 17°C are used to approximate the data at 13°C. This approximation is acceptable because the difference in recovery rate between 13°C and 17°C is probably similar to the variation in recovery rate among cells at a single temperature. Ionic currents are calculated as

$$I_{Na} = G_{Na}P_{open}(V - E_{Na}) \quad (11)$$

where I_{Na} is the sodium current, G_{Na} is the maximal channel conductance, P_{open} is the probability of occupying the open states ($O_1 + O_2$), V is the membrane potential, and E_{Na} is the reversal potential for sodium. G_{Na} is a function of temperature and thus is a parameter to be determined at both 13°C and 21°C. E_{Na} is dependent upon the experimental solutions, which are different for the data at 13°C and 21°C, and so is set accordingly at each temperature. Gating current is calculated according to the formula (Vandenberg and Bezanilla, 1991):

$$I_g = \sum_{jk} ne(z_{jk} + z_{kj})[P_j\lambda_{jk} - P_k\lambda_{kj}] \quad (12)$$

where n is the number of channels, e is the elementary charge unit, z is the effective valence, P_j is the probability of occupying state j, and λ_{jk} is the rate constant for the transition from state j to state k. Gating charge is found by integrating the gating current. Ionic currents and gating charge are computed using the following protocol. The membrane potential is held at −150 mV and then stepped for 20 ms to a potential between −70 mV and 20 mV inclusive in 10-mV increments. To eliminate convergence problems introduced by experimental error for potentials ≥−20 mV, gating charge accumulation curves are fit with a single exponential function and the curve fit values, instead of the experimental data, are used for the plateau portion of the gating charge accumulation curves. Tail currents are computed by stepping from −150 mV to 40 mV until the current reaches its maximal value (after 0.94 ms) and then stepping down to potentials between −150 mV and −90 mV inclusive in 10-mV increments for 5 ms. Recovery from inactivation is assessed using a double-pulse protocol. The membrane potential is held at −140 mV and then stepped to −20 mV for 1 s. The potential is then stepped down to either −100 mV or −140 mV for lengths of time varying from 5 to 600 ms. Current is then measured during a 4-ms step to 0 mV to assess the amount of recovery. Open time distributions are calculated for potentials between −90 and −10 mV inclusive in 10-mV increments using a simplified model in which all transitions out of the open states are to an absorbing non-open state. The simplified model and the equation for the open time distributions are shown in the Appendix. Each data set is weighted so that all sets have approximately the same influence on the cost function and so that the parameters determined by the algorithm are those parameters which best reproduce all of the channel kinetics. The weights for ionic current, gating charge, steady-state inactivation, tail current, recovery from inactivation, and open time cost function terms are 1, 250, 1, 500, 1000, and 5000, respectively.

The experimental data for 21°C include ionic currents (Wang et al., 1996), gating charge accumulation (Josephson and Sperelakis, 1992), the steady-state inactivation curve (Wang et al., 1996), the time course of recovery from inactivation (Wang et al., 1996), and single channel open times (Benndorf, 1988). To compute the ionic currents, the membrane potential is held at −120 mV and then stepped for 15 ms to a potential between −60 mV and 20 mV inclusive in 10-mV increments. The same protocol is used to compute gating charge accumulation except that the holding potential is −150 mV. From measurements of gating charge in squid giant axon, the maximum charge displaced at each potential does not vary with temperature (Jonas, 1989). Therefore, the model's computed maximum charge values for 13°C were used as the experimental charge values for 21°C. Recovery from inactivation is again measured using a double-pulse protocol. The holding potential is −120 mV and the test potential is −20 mV; recovery times are varied between 10 ms and 250 ms. Open time distributions are calculated for potentials between −70 and −20 mV inclusive in 10-mV increments. The weights for ionic current, gating charge, steady-state inactivation, recovery from inactivation, and open time cost function terms are 100, 10, 5000, 500, and 500, respectively.

Model testing

The single channel behavior of the model was tested, which required the state transitions to be determined using a stochastic approach (Clay and DeFelice, 1983). In this method, the length of time a channel stays in its current state (i.e., its dwell time, denoted as T_j) is calculated according to the formula

$$T_j = -(\ln r) \Big/ \sum_{k=1}^{x} \lambda_{jk} \quad (13)$$

where r is a random number from the uniform distribution [0, 1] and λ_{jk} is the transition rate from state j to state k. The sum is over the x pathways out of state j. At the end of the dwell time, the new state of the channel is determined by assigning random numbers to a portion of the interval [0, 1] based on the probabilities of changing to neighboring states. These probabilities are equal to the rate constant for a particular transition divided by the sum of the rate constants for all possible transitions. For example, a channel in state C_1 can transit to C_2 or C_1I. The probability of changing to C_2 is $4\alpha/(C_n + 4\alpha)$, where 4α is the rate constant for $C_1 \rightarrow C_2$ and C_n is the rate constant for $C_1 \rightarrow C_1I$. Once the new state is determined, another random number is used to calculate the dwell time in the new state. At an instantaneous voltage step, channels remain in their current state, but the dwell times are recalculated.

RESULTS

The model parameters determined to give the best total fit of model responses to experimental data for ionic currents, gating charge, steady-state inactivation, tail currents, recovery from inactivation, and open times are listed in Table 1. The rate constants governing the $O_1 \rightarrow C_4$ (deactivation) and the $O_1 \rightarrow I$ (inactivation) transitions have been measured experimentally. Benndorf and Koopmann found the enthalpies, entropies, and effective valences to be 129 kJ mol^{-1}, 0.23 kJ mol^{-1} K^{-1}, and 1.54 for deactivation and 79 kJ mol^{-1}, 0.10 kJ mol^{-1} K^{-1}, and 0.68 for inactivation, respectively (Benndorf and Koopmann, 1993). The model parameters are 128 kJ mol^{-1}, 0.229 kJ mol^{-1} K^{-1}, and 1.33 for deactivation and 62 kJ mol^{-1}, 0.039 kJ mol^{-1} K^{-1}, and 0.66 for inactivation, respectively. The model parameters for deactivation are very similar to the experimental data, whereas the parameters for inactivation differ slightly from the experimental data. The Gibbs free energies for inactivation for the experimental data and the model parameters, however, are very similar. Therefore, the discrepancy in

TABLE 1 Model parameters

Parameters	ΔH (J mol^{-1})	ΔS (J mol^{-1} K^{-1})	z
α	116,900	224.114	0
β	263,870	708.146	−0.9701
γ	200.240	529.952	1.5703
δ	127,970	229.205	−1.3266
O_n	62,385	39.295	0.6625
O_f	79,035	1.510	0
$\gamma\gamma$	−99,967	−578.317	0
$\delta\delta$	62,555	−130.639	−3.5596
ϵ	79,183	70.078	0
ω	123,020	225.175	0
η	150,333	338.915	1.5717
ν	121,900	193.265	−1.3281
C_n	293,270	786.217	0
C_f	57,533	0.00711	0

Markov model parameters determined by the simulated annealing minimization algorithm.

inactivation parameters probably results from the minimization algorithm not being able to discriminate between several pairs of enthalpy and entropy terms yielding the same Gibbs free energy.

To assess the sensitivity of the model parameters, each parameter is varied by $\pm 1\%$ of its value and the change in the cost function is computed. A change in the value of the Gibbs free energy produces a much larger change in the cost function than does a change in the value of the corresponding valence. Thus, the Gibbs free energies are much more sensitive to a change in their values than are the valences. This sensitivity difference can be attributed to the different importance Gibbs free energies and valences have in determining the rate constants. The Gibbs free energies are the larger of the two terms in the exponential function and therefore are mainly responsible for determining the rate constant. In contrast, the voltage-dependent terms serve only to slightly modify the basic rates set by the Gibbs free energies. Thus, by changing the Gibbs free energies, one can produce a much larger change in the rate constant and a much larger change in the cost function.

Changes in the enthalpy and entropy terms of α, β, and C_n produce the largest changes in the cost function. The total error increases by up to 10 times for a 1% change in these parameters. The large sensitivity of these parameters is probably due to their role in providing temperature dependence. Parameters α and β must have precise enthalpy and entropy terms in order to accurately describe the increased rate of channel activation and rate of recovery from inactivation with temperature. C_n requires precise enthalpy and entropy terms in order to describe the shift in the steady-state inactivation curve with temperature. At 13°C, a change in the enthalpy of ϵ also produces a large change in the cost function. However, at 21°C, the same change produces much less change in the cost function, because the probability of occupying the second open state is much lower at this temperature.

In contrast to the large sensitivity of α, β, C_n, and ϵ, a 1% change in the enthalpy and entropy terms of $\gamma\gamma$, $\delta\delta$, and O_f, as well as in the entropy term of C_f, produces almost no change in the total error. Two different explanations account for this small sensitivity. First, the entropies of O_f and C_f are a much smaller fraction of their respective enthalpies than are the entropies of other parameters. Thus, based on their relative size alone, one would expect a 1% change in their values to have little influence on the total error. Second, a change in the enthalpy and entropy terms of $\gamma\gamma$, $\delta\delta$, and O_f most likely produces little effect on the error because there is not enough information in the experimental data to adequately constrain two separate terms. This observation is in contrast to changing the Gibbs free energy term for these parameters, which does produce a measurable change in the total error. These results suggest that while the entropy and enthalpy terms of $\gamma\gamma$, $\delta\delta$, and O_f may not be well determined, the Gibbs free energy they define is. In other words, there may be several combinations of entropy and enthalpy terms that produce an appropriate Gibbs free energy for $\gamma\gamma$, $\delta\delta$, and O_f.

The parameter values can be used to assess the amount of charge moved with each transition in the model. The model parameters suggest that activation requires the movement of 6.8 charges and inactivation requires the movement of 0.66 charges. Estimates of the charge associated with activation usually range from 4 to 7 (Hodgkin and Huxley, 1952a; Oxford, 1981; Sheets and Hanck, 1995), although some researchers have found that at least 12 charges are needed (Hirschberg et al., 1995). Estimates of the charge associated with inactivation range from 0.75 to 1.9 charges (Horn et al., 1984; Vandenberg and Horn, 1984; Yue et al., 1989; Lawrence et al., 1991; Sheets and Hanck, 1995). Thus, the model's estimates of charges required for activation and inactivation are similar to values measured experimentally.

Most of the charge movement in the activation pathway is concentrated in the last transition ($C_4 \rightarrow O_1$ or $C_4 \rightarrow O_2$). This finding seemingly contradicts the hypothesis that the final transition in the activation pathway is voltage-independent for all voltage-gated channels. However, these transitions in the model probably represent several steps lumped together so that, in reality, the final step may really be voltage-independent (Kuo and Bean, 1994). Furthermore, gating currents, which depend heavily on the voltage-dependence of each transition, have only been used in developing a few models. In another sodium channel model developed using gating currents, the closed-to-open transition also has the greatest voltage dependence (Vandenberg and Bezanilla, 1991).

The model is able to reproduce a wide range of experimental data. Fig. 2 shows representative traces of the model-derived ionic current in comparison to the experimental data at 13°C (provided by Hanck and Sheets, similar to Sheets et al., 1996) and at 21°C (provided by Bennett, similar to Wang et al., 1996) for clamp voltages of −50 mV, −30 mV, −10 mV, and 10 mV. Although the peak current values deviate slightly from the experimental values, the time courses of activation and inactivation are generally well fit by the model at both temperatures. For potentials > -40 mV, the model-derived currents decay to zero within 50 ms, whereas the experimental currents do not. The model decays to zero faster than the experimental data at 13°C because the experimental data have both fast and slow components of inactivation, whereas the model has only fast inactivation.

Fig. 3 compares model-derived current-voltage relationships at 13°C (Fig. 3 *A*) and 21°C (Fig. 3 *C*) with experimental data used in the fitting process. Fig. 3 *B* compares the current-voltage relation predicted at 17°C with experimental data (provided by Wasserstrom, similar to Sakakibara et al., 1993). As shown by the current-voltage relationships, the model reproduces peak current well throughout the voltage and temperature range tested. At 13°C, the current magnitudes deviate most significantly from the corresponding experimental data over the voltage range −60 mV to −45 mV. In this range, the model produces less current than the experimental data. This reduction in current probably results from inactivation that is too fast, which reduces the number of channel reopenings.

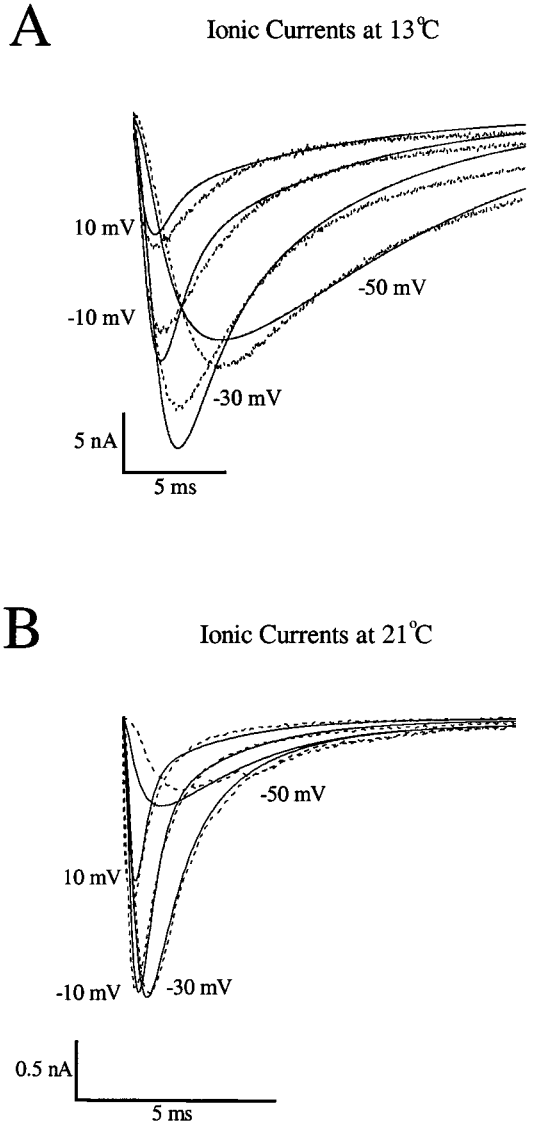

FIGURE 2 Comparison of voltage-clamped sodium current tracings for clamp voltages of −50 mV, −30 mV, −10 mV, and 10 mV for experimental data (*dashed lines*) and the model (*solid lines*). (*A*) At 13°C (experimental data provided by Hanck and Sheets similar to Sheets et al., 1996). (*B*) At 21°C (experimental data provided by Bennett similar to Wang et al., 1996).

At 17°C, peak currents also differ over this voltage range. Considering, however, that data at this temperature were not fit and were obtained from a different experimental preparation than any of the other data, the model reproduces the data well. At 21°C, peak currents are well fit except at very depolarized potentials. Both the model and experimental current-voltage curves are fit using a modified Boltzmann function

$$I = \frac{G_{Na}(V - E_{Na})}{1 + \exp\left(\frac{V - V_{0.5}}{s}\right)} \tag{14}$$

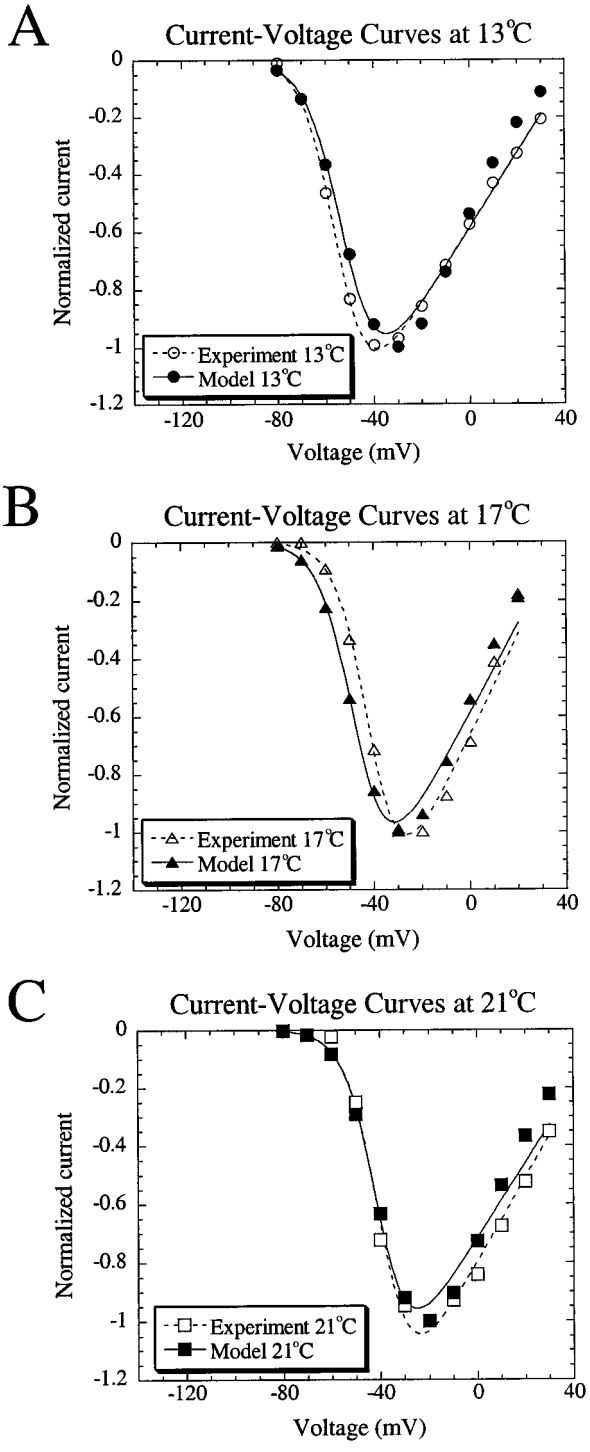

FIGURE 3 Normalized current-voltage curves for experimental data and the model. Curves are the best fits to Eq. 14 in the text. See Table 2 for fitted parameters. (*A*) At 13°C experimental data (○) and the model (●) (experimental data provided by Hanck and Sheets similar to Sheets et al., 1996). (*B*) At 17°C experimental data (△) and the model (▲) (experimental data provided by Wasserstrom similar to Sakakibara et al., 1993). (*C*) At 21°C experimental data (□) and the model (■) (experimental data provided by Bennett similar to Wang et al., 1996).

where G_{Na} is the conductance, V is the voltage, E_{Na} is the reversal potential, $V_{0.5}$ is the potential at which the current is half-maximal, and s is the slope factor. The resulting

parameters are listed in Table 2. The conductances and slope factors are similar with the model having a slightly shallower slope for 13°C and 17°C and a slightly steeper slope for 21°C. The model's half-maximal voltages differ from the corresponding experimental data by 3.1 mV, 6.1 mV, and 1.2 mV for 13°C, 17°C, and 21°C, respectively. This difference is reflected in the slightly rightward shift of the model's current-voltage curve for 13°C and the slightly leftward shift of the model's current-voltage curve for 17°C. The model shows a rightward shift of the half-maximal potential (11.2 mV per 8°C) as the temperature is increased. Rightward shifts in the half-maximal potentials of the steady-state activation (8 mV per 10°C) and inactivation curves (7 mV per 10°C) as the temperature is increased have been measured experimentally (Murray et al., 1990). These shifts would produce a shift in the current-voltage relationship similar to that produced by the model.

Fig. 4, *A* and *B* show the time to peak current and the time constants of inactivation for 13°C, 17°C, and 21°C. The model's time to peak current is very similar to the corresponding experimental data for all the voltages and temperatures tested. As the temperature is increased, the time to peak current is reduced, as expected from data in the literature (Colatsky, 1980; Murray et al., 1990). The time constants of inactivation are estimated by fitting an exponential function to the current decay. For potentials of −30 mV and greater, the model's ionic current decay is better fit with two exponentials. The experimental data also have a second exponential at these potentials. However, the time constant of this second exponential in the experimental data is too large to accurately determine with a voltage clamp of 35 ms. Therefore, in order to compare the model's time constants with those of the experimental data, a single exponential fit is used in Fig. 4 *B*. At 13°C, the inactivation time constants predicted by the model are larger than those of the experimental data at both ends of the voltage range, while they are similar to those of the experimental data in the middle of the voltage range. The discrepancy in the time constants at negative potentials is probably due to error in the fitting procedure as a result of having only two or three time constants' worth of data. In addition, the model's time constants increase for very depolarized potentials, whereas the experimental data show that the time constants decrease monotonically as voltage is increased. This apparent discrepancy is an artifact of fitting the model's decay with a single exponential. As the potential is increased, the model's decay switches from that described by a large fast component and a small slow component to one described by a small fast component and a large slow component. As the slower component becomes larger, the time constant determined by fitting a single exponential to the decay increases. If just the fast or slow time constant from a biexponential fit of the model's decay is plotted, the time constants do decrease monotonically with increasing voltage. At 17°C and 21°C, the model's time constants of inactivation are similar to the corresponding experimental data. As the temperature is increased, the time constants become faster, as expected from data in the literature (Colatsky, 1980). Thus,

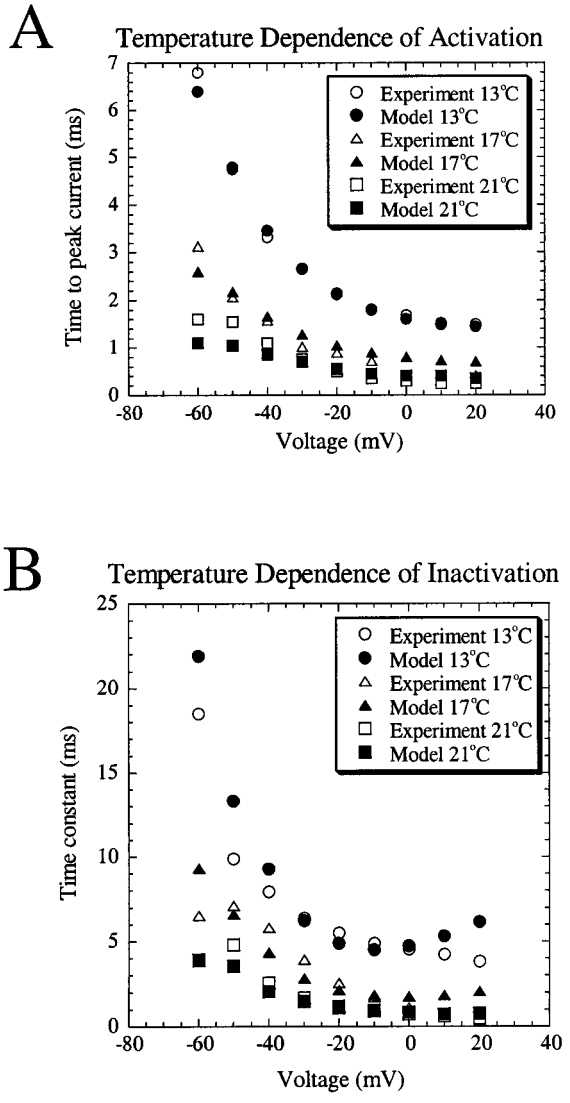

FIGURE 4 Temperature dependence of activation and inactivation at 13°C (experimental data (○), model (●)), at 17°C (experimental data (△), model (▲)), and at 21°C (experimental data (□), model (■)). Experimental data from sources listed in Fig. 3. (*A*) Time to peak current. (*B*) Time constants of inactivation determined by fitting a single exponential to the current decay.

TABLE 2 Boltzmann parameters for the current-voltage curves

	E_{Na} (mV)	G_{Na} (mV^{-1})	$V_{0.5}$ (mV)	Slope factor (mV)
Experiment 13°C	44.675	0.0131	−55.045	−6.734
Model 13°C	44.675	0.0132	−51.962	−7.450
Experiment 17°C	38.020	0.0174	−41.006	−6.640
Model 17°C	38.020	0.0154	−47.106	−7.002
Experiment 21°C	55.000	0.0145	−39.603	−6.748
Model 21°C	55.000	0.0130	−40.750	−6.604

Parameters of Eq. 14 that fit the current-voltage curves for the experimental data and the model at 13°C, 17°C, and 21°C.

the model reproduces well the activation and inactivation properties of the channel for a large voltage and temperature range.

The second data set reproduced by the model is gating charge movement in response to voltage-clamp stimuli. Fig. 5 *A* shows a comparison of the charge-voltage curves for the model and the experimental data (provided by Hanck and Sheets, similar to Sheets et al., 1996) at 13°C. The magnitudes plotted here for the model are the maximum charge accumulated at 30 ms. Some error is associated with these values because charge is still being accumulated at a very slow rate at 30 ms; that is, in the model, the plateau portion of the charge accumulation curves is not completely flat, but rather has a small slope. The nonequilibrium movement of charge is most likely due to constraints imposed by microscopic reversibility on the closed-open-inactivated loop. Nevertheless, the magnitude of charge movement is well reproduced by the model over most of the voltage range tested. Fitting a Boltzmann function to the experimental data at 13°C yields slope factor and half-maximal potential values of 15.7 mV and −63.3 mV. However, the experimental data for −70 mV and −60 mV appear to deviate significantly from the remainder of the data. Exclusion of these two points results in a better fit (correlation coefficient 0.996 versus 0.984). The slope factor and half-maximal potential values for this fit are 15.8 mV and −70 mV. The model's half-maximal potential is identical to that of the experimental data (−70 mV) and its slope is slightly steeper (14 mV). Fig. 5 *B* compares the model's charge-voltage curves for 13°C and 21°C. At 21°C, maximum charge values are taken at 20 ms even though charge is still being accumulated at a very slow rate. Fitting a Boltzmann function to the 21°C curve yields slope factor and half-maximal potential values of 19.6 mV and −63.9 mV, respectively. Thus, with increased temperature, the charge-voltage curve shifts rightward by 6.1 mV per 8°C. Although data on the temperature dependence of the charge-voltage curve for heart tissue have not been published, Hanck and co-workers have shown that the charge-voltage curve, although having a steeper slope, is similar to the peak sodium conductance curve (Hanck et al., 1990). Thus, one would expect the charge-voltage curve to be shifted rightward with increasing temperature since the peak sodium conductance curve is shifted rightward with temperature (Murray et al., 1990). Therefore, the model can reproduce the charge-voltage relationship over a large range of voltages and temperatures.

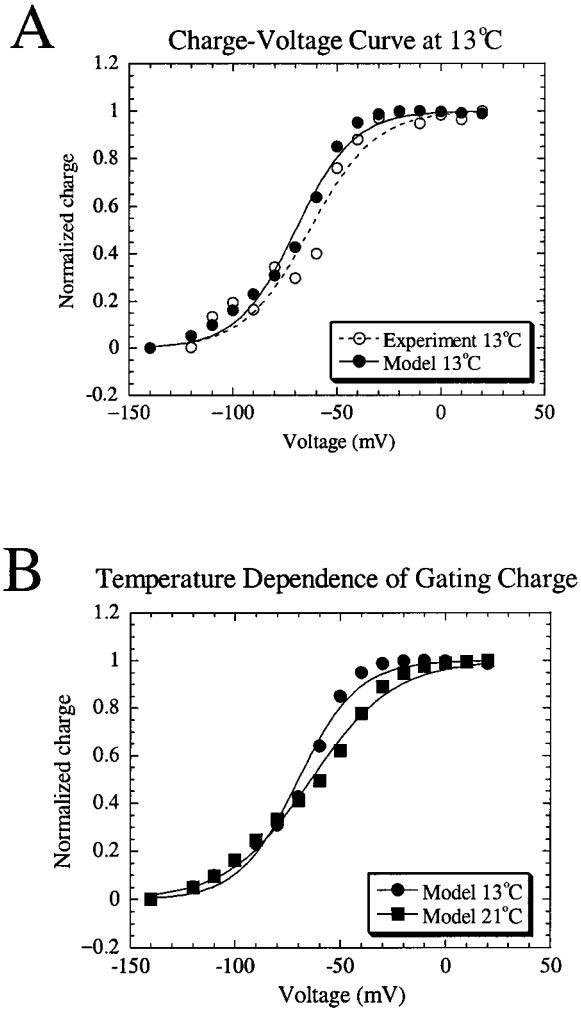

FIGURE 5 Normalized gating charge-voltage curves. (*A*) At 13°C for experimental data (○) (provided by Hanck and Sheets similar to Sheets et al., 1996) and the model (●). Curves are the best fits to a Boltzmann function where the slope factor and half-maximal potential values are 15.7 mV and −63.3 mV for the experimental data and 14.0 mV and −70 mV for the model, respectively. (*B*) Model's charge-voltage curves at 13°C (●) and at 21°C (■). The slope factor and half-maximal potential values for 21°C are 19.6 mV and −63.9 mV, respectively.

The model can also approximate the rate of gating charge movement. Fig. 6 shows the gating charge accumulation time constants as a function of voltage for the model and experimental data (provided by Hanck and Sheets, similar to Sheets et al., 1996) at 13°C and for the model at 21°C. For potentials ≥−50 mV, gating charge accumulation is well fit by a single exponential. For potentials <−50 mV, the model's gating charge accumulation curves exhibit an initial

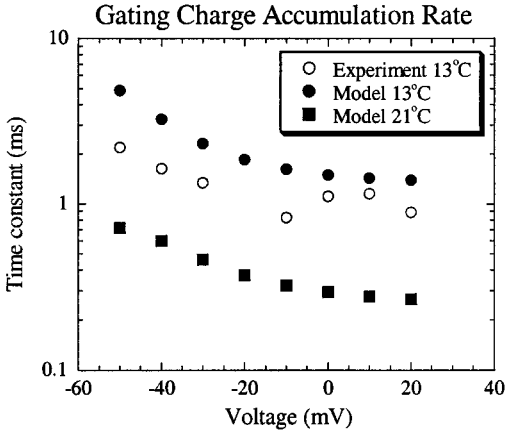

FIGURE 6 Time constants of gating charge accumulations (experimental data at 13°C (○), model data at 13°C (●), model data at 21°C (■)). Experimental data from source listed in Fig. 5.

fast decay followed by a much slower return to zero. Since the gating charge accumulation is thus not well fit by a single exponential, these potentials were excluded from Fig. 6. Note that the experimental time constants plotted in Fig. 6 are those obtained from a single measurement of gating charge from one cell and are from a different cell than the ionic currents. Taking these facts into consideration, at 13°C, although the model has larger time constants at each potential, it approximates the voltage dependence of these time constants reasonably well. At 21°C, one would expect the time constants of gating charge accumulation to be much faster (Josephson and Sperelakis, 1992) and the model meets this expectation with ~1 ms reduction in the time constants throughout the voltage range.

A third data set reproduced by the model is steady-state availability. Fig. 7 *A* shows the steady-state availability curves for the model and the experimental data (provided by Hanck and Sheets) at 13°C. The model's curve is nearly identical to that of the experimental data as reflected in the slope factor and half-maximal potential values of the respective Boltzmann functions. For the experimental data, the slope factor and half-maximal potential values are −9.9 mV and −106.1 mV. For the model, the respective values are −10.6 mV and −107 mV. Fig. 7 *B* compares the steady-state availability curves at 13°C and 21°C. At 21°C, there is a noticeable rightward shift of the curve. Fitting a Boltzmann function to the 21°C curve yields slope factor and half-maximal potential values of −15.2 mV and −101.7 mV. Thus, as the temperature is increased, the model produces a rightward shift of 5.3 mV per 8°C. This shift is similar to that measured experimentally, which is 7 mV per 10°C (Murray et al., 1990). Experimental data also predict that the slope factor increases slightly (0.5 mV per 10°C) over the temperature range 16°C to 26°C (Murray et al., 1990). The additional increase in slope factor over that predicted by the experimental data probably results from the exponential form of the rate constants, which prevents them from becoming constant except at the extremes of the voltage range. The nonsaturating rate constants prevent a true plateau of the curve at very negative potentials and thus, as temperature is increased, the curve cannot simply be shifted to the right. Nevertheless, the model is able to reproduce well the level of inactivation over a large voltage and temperature range.

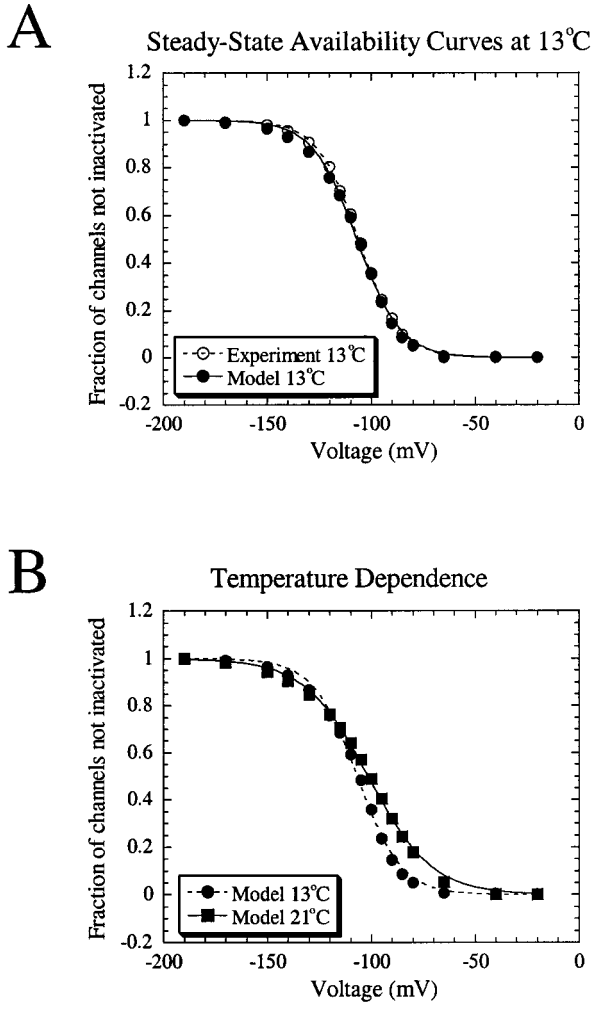

FIGURE 7 Steady-state availability curves. (*A*) At 13°C for experimental data (○) (provided by Hanck and Sheets similar to Sheets et al., 1996) and the model (●). Curves are the best fits of a Boltzmann function where the slope factor and half-maximal potential values are −9.9 mV and −106.1 mV for the experimental data and −10.6 mV and −107 mV for the model, respectively. (*B*) Model's steady-state availability curves at 13°C (●) and at 21°C (■). The slope factor and half-maximal potential values for 21°C are −15.2 mV and −101.7 mV, respectively.

In addition to ionic currents, gating charge, and steady-state availability, the model can reproduce recovery from inactivation. Shown in Fig. 8 *A* is the rate at which the model recovers from inactivation at 13°C in comparison to experimental data (Sakakibara et al., 1993). The model recovers from inactivation at a similar rate as the experimental data for a holding potential of −100 mV and, as the holding potential is decreased, the model recovers faster. For −100 mV, both the experimental data and the model show a delay of 10 ms before recovery occurs. Sakakibara and co-workers fit the experimental data using the sum of two exponentials. However, their data can be fit just as well with a single exponential, and this form yields better fits to the model results. For −100 mV the time constants are 164.9 ms and 177.7 ms, for −120 mV they are 42.9 ms and 46.7 ms, and for −140 mV they are 6.9 ms and 21.9 ms for the experimental and model data, respectively. The model's time constants are generally larger than those of the experimental data and, as the holding potential is decreased, the difference between the time constants increases. One possible explanation for the model's recovery rate being too slow is a lack of voltage dependence of the rate constants governing transitions between the closed and closed-inactivated states. Adding voltage dependence here could allow the model to more correctly approximate the time constant of recovery as holding potentials are lowered, but such a change would increase model complexity substantially by adding additional loops for which microscopic reversibility must be satisfied. Fig. 8 *B* compares the rates of recovery

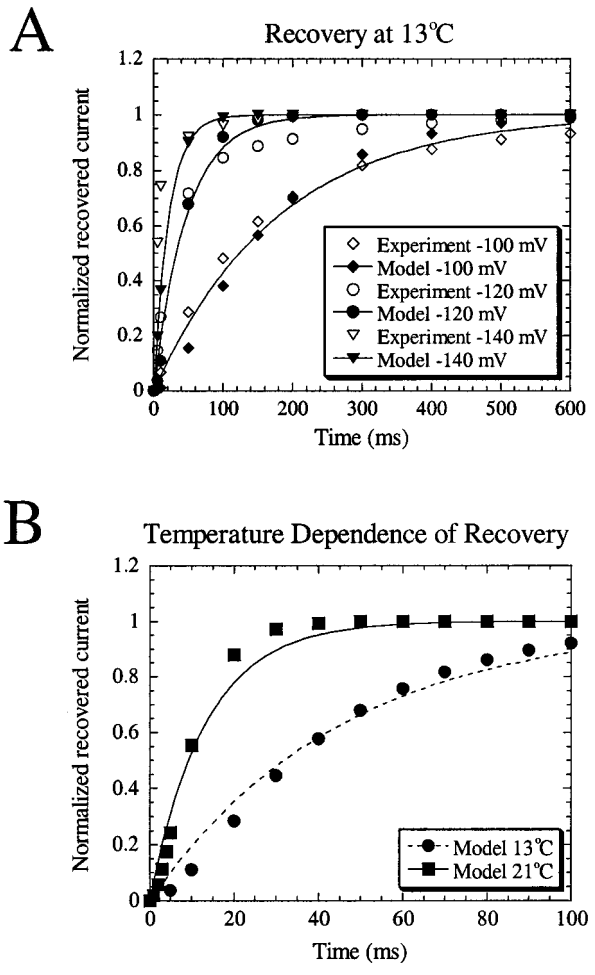

FIGURE 8 Rates of recovery from inactivation. (*A*) At 13°C for experimental data (Sakakibara et al., 1993) and the model. Data are plotted for holding potentials of −100 mV (experimental data (◇), model (◆)), −120 mV (experimental data (○), model (●)), and −140 mV (experimental data (▽), model (▼)). Model curves are fit using a single exponential with time constants of 177.7 ms, 46.7 ms, and 21.9 ms for −100 mV, −120 mV, and −140 mV, respectively. (*B*) Model's recovery from inactivation curves for a holding potential of −120 mV at 13°C (●) and 21°C (■). The time constant at 21°C is 13.3 ms.

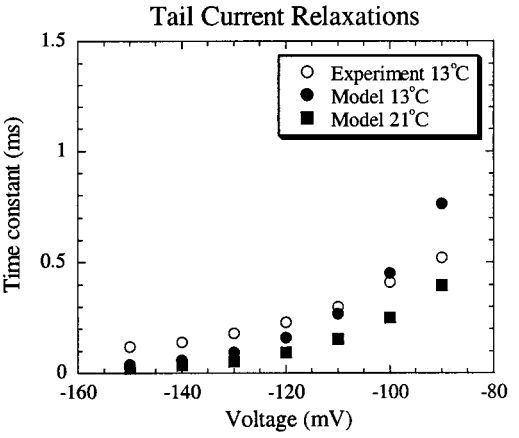

FIGURE 9 Time constants from a single exponential fit of the tail current relaxations at 13°C for experimental data (Hanck and Sheets, 1995) (○) and the model (●) and at 21°C for the model (■).

from inactivation at 13°C and 21°C for a holding potential of −120 mV. As temperature is increased, the recovery rate is increased significantly. Fitting a single exponential to the recovery data at 21°C yields a time constant of 13.3 ms. This rate is similar to that found by refitting published data at 21°C (Wang et al., 1996) with a single exponential, which yields a time constant of 15 ms. The model presented here thus differs from existing Markov models of the cardiac sodium channel (Benndorf, 1988; Berman et al., 1989; Scanley et al., 1990) in that it recovers from inactivation with the correct voltage dependence.

The model also reproduces the rate at which an open channel deactivates. Plotted in Fig. 9 are the time constants from a single exponential fit of the current decay at 13°C upon stepping from 40 mV to the test potential. The model has two deactivation pathways ($O_1 \rightarrow C_4$ and $O_2 \rightarrow C_4$) and therefore will have a biexponential tail current. For potentials of −100 mV and below, the model's time constants are similar to those measured experimentally (Hanck and Sheets, 1995) and there is little difference between a monoexponential and a biexponential fit to the data. At these potentials, the $O_1 \rightarrow C_4$ pathway, which is faster, appears to dominate. At more depolarized potentials, the model predicts larger time constants than measured experimentally and the current decay is much better fit using two exponentials. Thus, as the test potential is increased, channels more readily exit the open states using both deactivation pathways. At 21°C, the current decay produced by the model is best fit using a single exponential at all potentials. At this temperature, the $O_1 \rightarrow C_4$ pathway dominates because of the low probability of occupying the second open state. As expected, as the temperature is increased, the rate of deactivation increases.

The final data set used to determine the model parameters is single channel open durations. Fig. 10 shows the model's densities of single channel open durations for both 13°C and 21°C. Twelve hundred channels are simulated, as described in Methods, for a 40-ms sweep and their open durations measured. At 13°C, for a clamp voltage of −50 mV, a histogram of open durations shows a wide variation of open times including a significant fraction >2 ms. In contrast, for a clamp voltage of −15 mV at 13°C, most of the channels have open times of <2 ms. These densities are clearly biexponential because the model has two open states and the dwell times in each open state are significantly different. At 21°C, for both clamp potentials, almost all of the channels have open times of <2 ms, but the densities are still biexponential. Experimental data for the densities and distributions of open times are usually fit with a single exponential. In order to compare the model and the experimental data, the distributions are calculated from Eq. A14 and are fit with a single exponential. Fitting the densities calculated from stochastic channel simulations yields the same results.

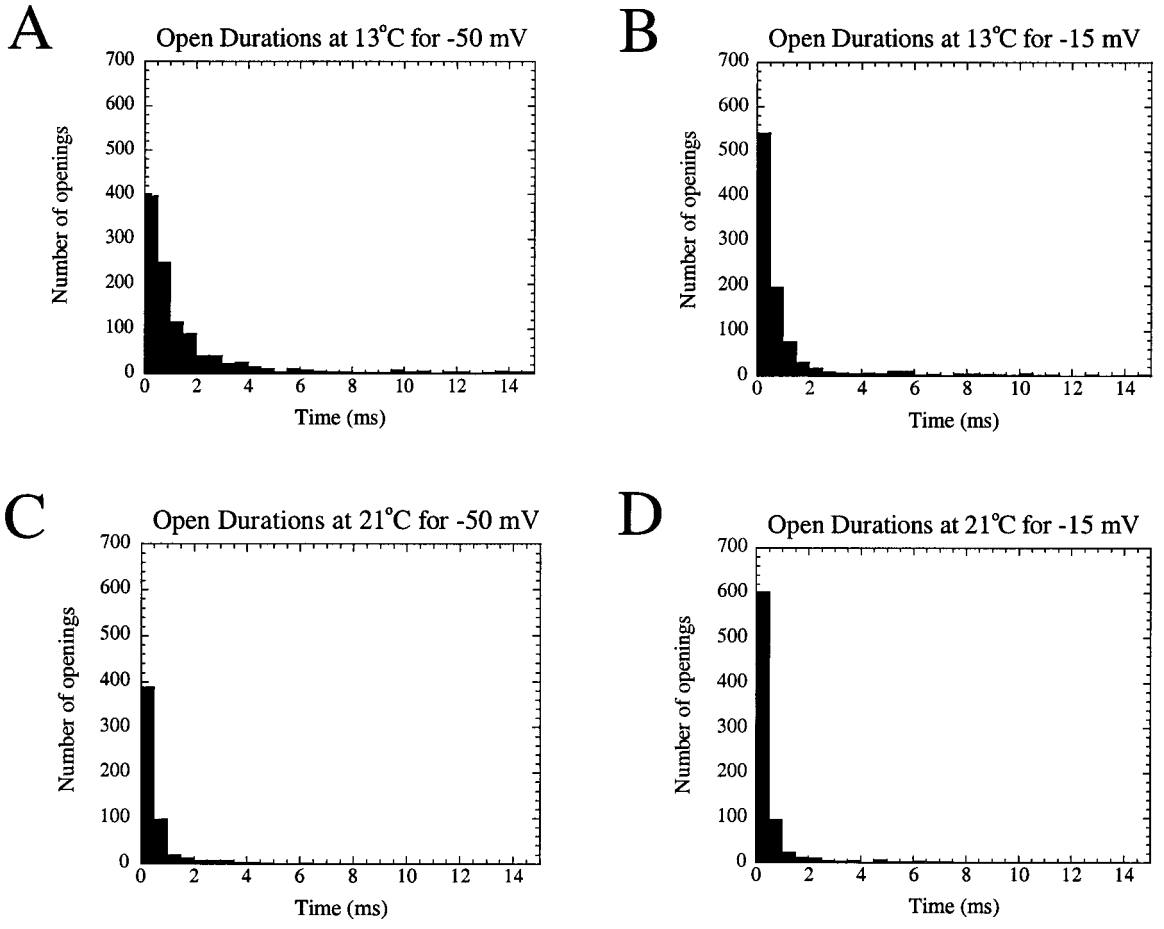

FIGURE 10 Densities of single channel open durations. Twelve hundred channels are simulated for 40 ms as described in the text. Bin size is 0.5 ms. (*A*) At 13°C for −50 mV. (*B*) At 13°C for −15 mV. (*C*) At 21°C for −50 mV. (*D*) At 21°C for −15 mV.

Fig. 11 shows the open time distribution time constants versus voltage at 13°C and 21°C and the model's prediction at 17°C. Experimental data by Scanley et al. (1990) are plotted for 13°C and by Benndorf (1988) for 21°C. For the entire voltage and temperature range depicted, the model data agree well with the experimental data. As temperature is increased, the model's open times become shorter and the peak open time is shifted rightward, both of which are supported by the experimental data. It should be emphasized that time constants obtained by fitting a single exponential to the open time distributions are not equal to the mean open times of the model. (The mean open times can be calculated using the probability density function in Eq. A13.) The mean open time at each potential is larger, particularly at very depolarized potentials, due to rare long occupancies of the second open state (see Fig. 10). Despite its larger mean open times, the model reproduces the distributions of the open durations well for a large voltage and temperature range.

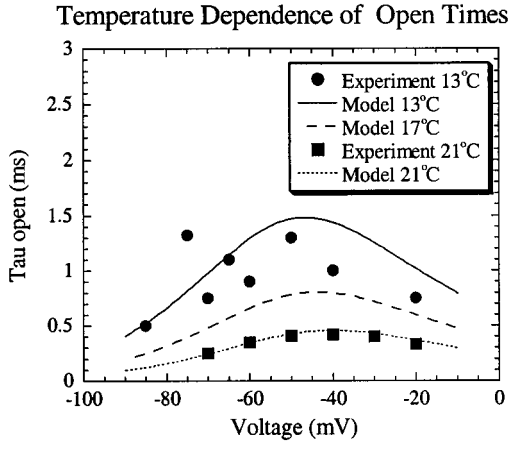

FIGURE 11 Model-predicted time constants for the open time distributions calculated from Eq. A14 at 13°C (*solid line*), 17°C (*dashed line*), and 21°C (*dotted line*). Experimental data by Scanley et al. (1990) (●) at 13°C and by Benndorf (1988) (■) at 21°C are also plotted.

The majority of the data presented to this point were used to determine the model's parameters. While it is important that the parameters adequately reproduce all the data used to determine them, it is also important that the parameters can be used to predict data not used in the fitting process. The ability of the model to fit data not used in determining the parameters is an independent test of how well the model

approximates reality. In developing the model, ionic currents obtained with different voltage clamp protocols were used. The model was thus constructed so that it could reproduce the ensemble behavior of many sodium channels. In testing the model, therefore, measures of single channel behavior were chosen to see if the model could represent one channel as well as the average of many channels.

Fig. 12 shows the first latency densities for clamp potentials of −50 mV and −15 mV at 13°C and 21°C. Single channel simulations are done as described previously. At 13°C, for a clamp voltage of −50 mV, there is a wide variation of first latencies with many longer than 10 ms. In contrast, for a clamp voltage of −15 mV at 13°C, almost all of the channels have first latencies of <5 ms. The probability that a channel first opens after time t was computed from these histograms and plotted versus time. The plots have a nonzero plateau that describes the probability of not opening during the channel simulation as well as a single time constant with which the probability relaxes to this plateau value. The plateau and time constant values are 0.34 and 6.41 ms for −50 mV and 0.22 and 1.65 ms for −15 mV, respectively. At 21°C, for a clamp voltage of −50 mV, a much larger fraction of channels have first latencies <5 ms, although there is still a wide variation in latencies. For −15 mV, almost all of the latencies are <2 ms. The plateau and time constant values at 21°C are 0.76 and 3.69 ms for −50 mV and 0.52 and 0.63 ms for −15 mV, respectively. Experimental data at 21°C for a clamp potential of −50 mV yield a time constant of 1.15 ms (Berman et al., 1989). The corresponding plateau value is not available. The model probably has a larger time constant because of the wide variation in the latencies. The long latencies are due to channels inactivating from a closed state for a considerable time and then returning to a closed state from which the channel can then open. The long latencies might be eliminated by adding voltage dependence to the transitions between the closed and closed-inactivated states. However, as discussed previously, such a change would greatly increase the complexity of the model. Although experimental data with which to compare the model's data are limited, first latencies are related to the time to peak current and thus, like these values, should decrease with temperature at all voltages, as the model predicts.

Finally, the model is used to predict the fraction of channels that do not open and the number of channels that reopen during a voltage clamp of 40 ms as additional tests

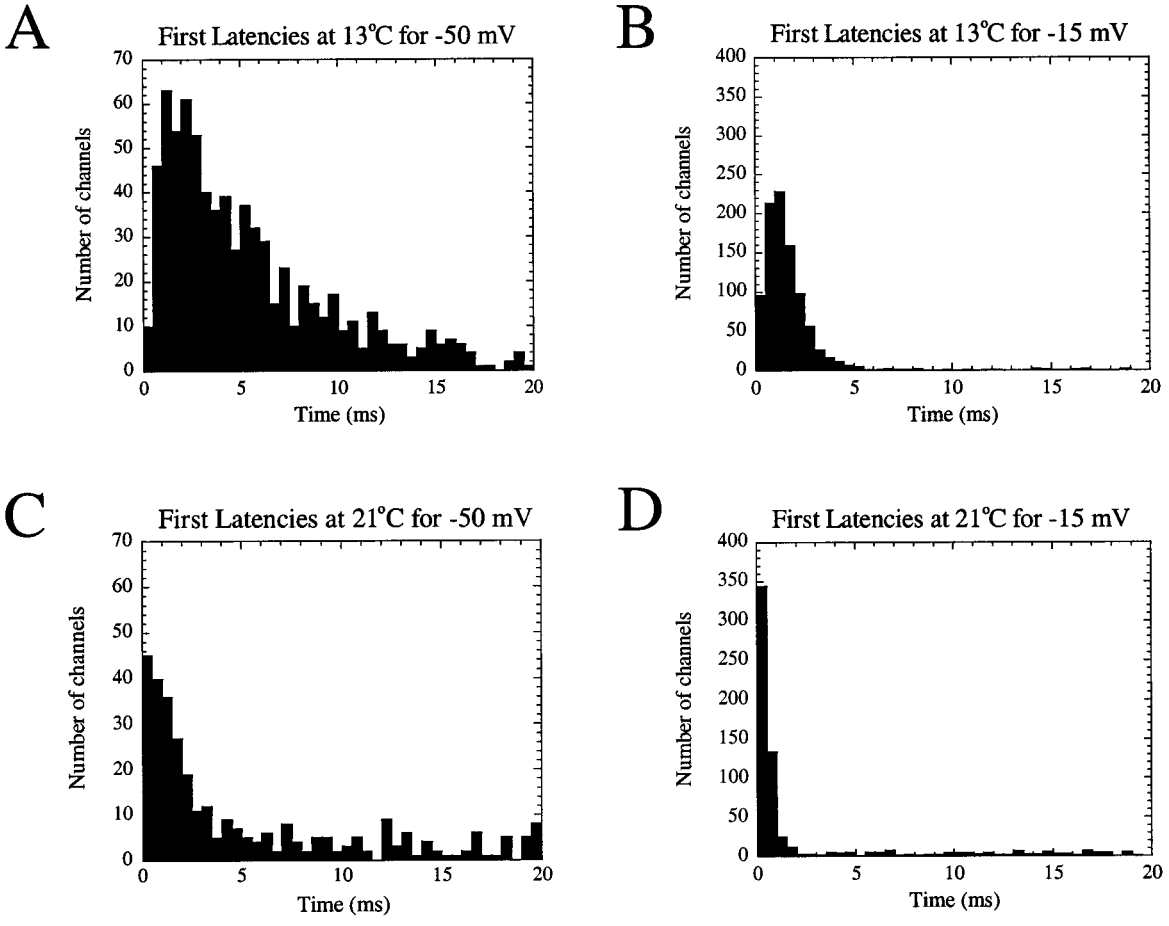

FIGURE 12 Densities of single channel first latencies. Twelve hundred channels are simulated for 40 ms as described in the text. Bin size is 0.5 ms. (*A*) At 13°C for −50 mV. (*B*) At 13°C for −15 mV. (*C*) At 21°C for −50 mV. (*D*) At 21°C for −15 mV.

of the model's ability to predict single channel behavior. Fig. 13 *A* shows the probability of not opening as a function of voltage at 13°C and 21°C. The probability of not opening is high at very negative potentials, while it is much lower at depolarized potentials. Even at these depolarized potentials, though, there is still a significant fraction of channels that do not open at both temperatures. The model's predictions for 13°C are generally lower than the experimental data reported by Scanley et al. (1990), although the overall trend of the curve is similar. The tendency for the model to predict slightly lower probabilities than those measured experimentally may be due to brief and missed openings in the experimental data. Experimentally, openings shorter than 178 μs cannot be detected (Scanley et al., 1990). If these openings are excluded from the model simulation, the resulting probabilities of a null sweep are increased by 5–20% depending on the clamp potential. The probability a channel does not open increases as the temperature is increased, as expected from data in the literature (Correa et al., 1992). This result suggests that as the temperature is increased, a larger fraction of channels are inactivated before they reach the open state.

Fig. 13 *B* shows the number of channel openings, normalized by the number of channels that open, versus voltage. At 13°C, there are a significant number of reopenings for −60 mV and −50 mV with the number of reopenings decreasing as the potential is increased. The model predicts that 32% of opening events are reopenings at −60 mV. This percentage is similar to that of the experimental data; by Scanley's calculations, at −57 mV, 39% of opening events are reopenings (Scanley et al., 1990). While the exact number of reopenings differs from Scanley's measurements, the overall trend of the curve is nevertheless similar. As the temperature is increased from 13°C to 21°C, the number of reopenings generally decreases and the peak of the reopening curve is shifted to the right. At 21°C a channel spends less time in the open state, and thus has less opportunity to close and reopen. These results are consistent with the reduction in open time and shift of the open time curve rightward as temperature is increased. Therefore, not only does the model fit well the ensemble channel behavior used to constrain the parameters, but it also predicts single channel behaviors not used in the fitting process.

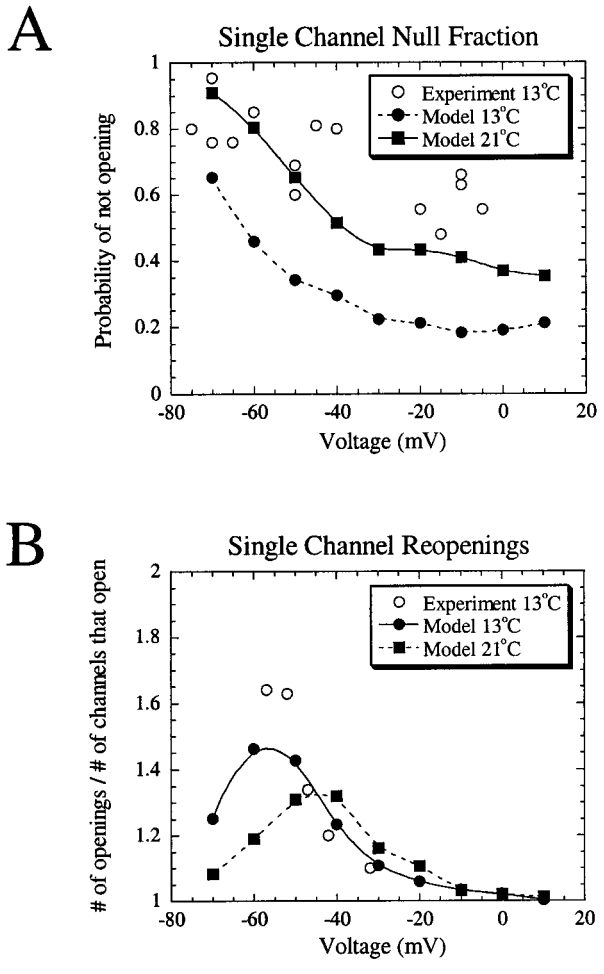

FIGURE 13 Single channel probabilities for experimental data (○) at 13°C (Scanley et al., 1990), model data at 13°C (●), and model data at 21°C (■). (*A*) The probability of not opening versus clamp voltage. (*B*) The number of channel openings, normalized by the number of channels that open, versus clamp voltage.

DISCUSSION

Three Hodgkin-Huxley models have been formulated to describe the kinetics of cardiac sodium channels. They are the Beeler-Reuter model (Beeler and Reuter, 1977), the Ebihara-Johnson model (Ebihara and Johnson, 1980), used in the Luo-Rudy ventricular cell model (Luo and Rudy, 1991), and the DiFrancesco-Noble model (DiFrancesco and Noble, 1985). All of these models were constructed by fitting empirically derived mathematical functions to channel activation and inactivation data. They all reproduce ionic currents in response to voltage clamp protocols and reproduce recovery from inactivation. As evidenced by their widespread use, these models are considered to provide accurate representations of the ensemble-average behavior of cardiac sodium channels.

The Markov model reported in this paper reproduces the same range of experimental data as that reproduced by these Hodgkin-Huxley models. In addition, the Markov model has two advantages over previous Hodgkin-Huxley models. First, the rate constants are not empirical functions, but rather are based on the thermodynamic principles of Eyring rate theory (Hille, 1992). This formulation gives physical meaning to the rate constants, allows a direct comparison of certain rate constants to experimental data, and facilitates the explicit incorporation of temperature dependence into the model. Second, the Markov model, as shown in Results, cannot only reproduce ensemble-average behavior, but can also predict single channel behaviors. The Beeler-Reuter, Ebihara-Johnson, and DiFrancesco-Noble models, in their original formulations, were intended only to represent channel ensemble behavior, not that of individual channels.

These Hodgkin-Huxley models can be expanded to have multiple resting and inactivated states, and thus can be made to represent a single channel. However, it is unclear whether such an expanded Hodgkin-Huxley model would predict these single channel behaviors as well as the Markov model. Studies done to compare the predictive ability of expanded Hodgkin-Huxley models versus Markov models are contradictory. Chay compared a five-state Markov model with an eight-state Hodgkin-Huxley model, both of which had absorbing inactivated states, and found that the Hodgkin-Huxley model was not inferior to the Markov model in its ability to predict single channel behaviors (Chay, 1991). However, this result differs from that of Horn and Vandenberg, who compared a five-state Markov model with a five-state Hodgkin-Huxley model. They found that the Hodgkin-Huxley model was not able to predict single channel behaviors as well as the Markov model (Horn and Vandenberg, 1984). In any case, multi-state models clearly have an advantage over the original Hodgkin-Huxley models in their ability to predict single channel behaviors. The Markov model in this paper therefore reproduces a wider range of experimental data than Hodgkin-Huxley models, and is thus a more complete representation of the cardiac sodium channel.

The new Markov model improves on existing Markov models of the cardiac sodium channel (Benndorf, 1988; Berman et al., 1989; Scanley et al., 1990) as well. These models were constructed to reproduce a subset of single channel data. To this end, they were made to have four or five states. They were not meant to closely resemble channel structure. In contrast, the Markov model reported here more closely follows the current hypotheses of channel structure. The model is similar to that proposed by Kuo and Bean for sodium channels in CA1 hippocampal neurons (Kuo and Bean, 1994). It is designed so that each closed and closed-inactivated state represents a specific combination of the positions of the four voltage sensors and the position of the inactivation particle (Hille, 1992). Having a model that follows the channel structure as closely as possible is important because it facilitates investigations of the structure-function relationship.

The Markov model reported here also improves on existing Markov models of the cardiac sodium channel because it can recover from inactivation. Previous Markov models of the cardiac sodium channel have an absorbing inactivated state and thus cannot recover from inactivation. Recovery from inactivation is necessary for any model to be used in studies of antiarrhythmic drug action. Antiarrhythmic drugs exhibit use-dependence, a property thought to determine their effectiveness (Hondeghem and Katzung, 1977; Starmer et al., 1984), that requires the application of a pulse train to measure. Models with an absorbing inactivated state cannot reproduce channel activity in response to a pulse train and thus will not reproduce use-dependence. Therefore, the Markov model reported here improves on previous Markov models of the cardiac sodium channel by more closely resembling the channel's structure and by reproducing recovery from inactivation.

There are two features of the Markov model in this paper that differ from Kuo and Bean's model (Kuo and Bean, 1994) and are necessary to model the cardiac isoform of the sodium channel. First, although many neuronal models are able to reproduce ionic currents assuming voltage-independent open-inactivated transitions, such is not the case with the model presented here. The open-inactivated transitions are associated with the movement of 0.66 charges. This value is close to the range of 0.75 to 1.9 charges reported for these transitions by others (Horn et al., 1984; Vandenberg and Horn, 1984; Sheets and Hanck, 1995). Sheets and Hanck (1995) measure a significant component of gating current due to this transition. The inclusion of voltage-dependent open-inactivated transitions is also supported by Yue, Lawrence, and co-workers' finding that voltage dependence is necessary to produce the correct voltage dependence of channel reopenings and mean open times (Yue et al., 1989; Lawrence et al., 1991). Without voltage dependence of the $O \rightarrow I$ transition, the mean open times increase monotonically as a function of voltage, instead of reaching a peak and then decaying.

A second difference from the model of Kuo and Bean is that the present model has two open states with the same conductance. This addition provides a second pathway by which the channel can open ($C_4 \rightarrow O_2$) and yields a better fit to the current decay by providing a temporary store of channels in the open state. Upon entering state O_1 the channel can either inactivate immediately or transition to O_2 before inactivating through O_1. To show the difference between a single open state model and a two open state model, a single open state model was developed at 13°C using the same procedure as described in Methods for the two open state model. Fig. 14 *A* compares several ionic currents from this single open state model with those of the experimental data. While the data for −50 mV are very similar, the model's decay is much too fast for all the other potentials. In addition, the model does not decay to zero, but rather to some plateau level of current. These plateaus are the result of trying to fit the decay without greatly increasing the open times (Fig. 14 *B*). A comparison of the single open state model results to those of the two open state model (Figs. 2 *A* and 10) shows that the two open state model does a much better job of reproducing the experimental data. Previous models of the cardiac sodium channel have had only a single open state because single channel open time distributions are well fit by a single exponential decay (Patlak and Oritz, 1985; Berman et al., 1989; Scanley et al., 1990). However, single channel open time distributions can also be well fit by multiple exponentials, particularly in the presence of toxins (Kunze et al., 1985; Nagy, 1987; Schreibmayer and Jeglitsch, 1992; Correa and Bezanilla, 1994). These toxins may be exposing open states that are always present but not readily distinguishable except in the presence of toxin. A second open state is also supported by the biexponential decay of the tail currents, which, in the

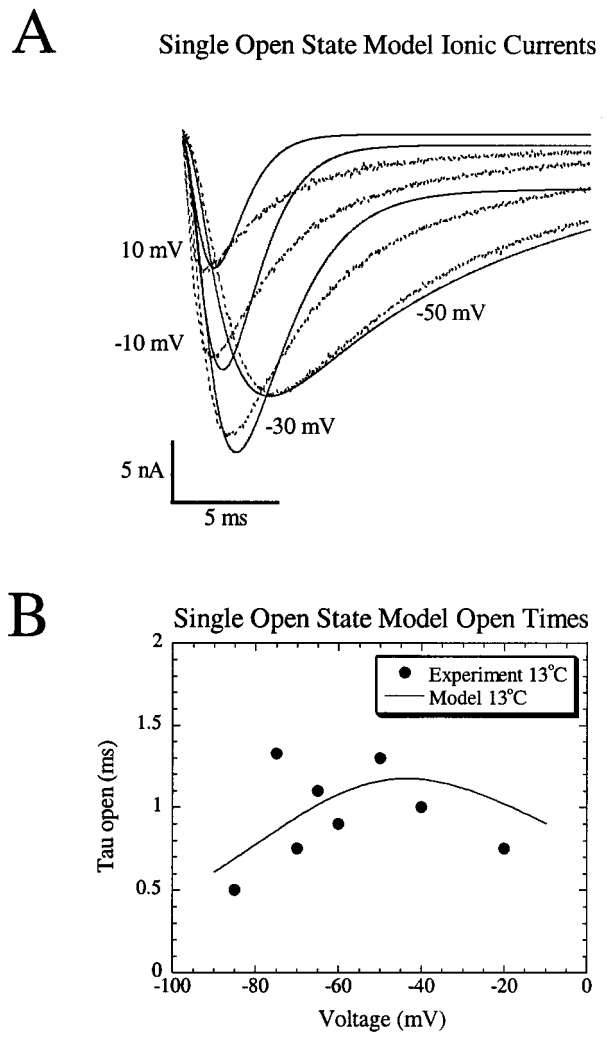

FIGURE 14 Single open state model results at 13°C. (*A*) Comparison of voltage-clamped sodium current tracings for clamp voltages of −50 mV, −30 mV, −10 mV, and 10 mV for experimental data (*dashed lines*) and the model (*solid lines*). (*B*) Model-predicted time constants of the open time distribution (*solid line*) compared to experimental data by Scanley (●) (Scanley et al., 1990).

absence of a two-step deactivation in which the first transition is a fast equilibrium and the second is slow, requires two pathways for deactivation and thus two open states (Elinder and Arhem, 1997). Additional transitions from O_2 directly to an inactivated state could have been added, but these transitions added unnecessary, ill-constrained parameters. The decay could also be fit using an additional inactivated state, but such a model requires the channel to reopen from the inactivated state throughout the voltage range tested in order to fit the data. From single channel studies, it is known that such reopening does not occur for very depolarized potentials (Berman et al., 1989; Scanley et al., 1990). Therefore, the addition of a second open state and voltage dependence to the open-inactivated transitions are modifications which are unique to modeling of the cardiac sodium channel isoform and are necessary to reproduce a full range of channel activity.

A final feature of the Markov model presented here that provides an advantage over previous models is its ability to reproduce experimental data over a range of temperatures. Hodgkin-Huxley models can be made to reproduce channel activity at multiple temperatures by modifying the conductance and the time constants of activation and inactivation by a Q_{10} factor and by shifting the steady-state activation and inactivation curves (Colatsky, 1980; Murray et al., 1990; Milburn et al., 1995). However, such models still have the disadvantages, which were discussed previously, of any Hodgkin-Huxley model as compared to the Markov model in this paper. No Markov models exist for sodium channels that can reproduce ensemble-average and single channel behaviors over a range of temperatures. To do so, each term in the model's rate constants needs to have its own temperature dependence or its own Q_{10} factor (Kohlhardt, 1990). Formulating the rate constants as exponential functions of the change in enthalpy and entropy allows the Markov model presented here to have explicit temperature dependence. As shown in Results, this formulation yields a model that reproduces ensemble-average and single channel behavior over a temperature range of 10°C to 25°C. A model with explicit temperature dependence is advantageous in characterizing a channel's behavior because it allows predictions to be made about how drugs or toxins differentially affect channel states as the temperature is changed. Therefore, the explicit temperature dependence of the Markov model presented here is an additional improvement on all previous models of the cardiac sodium channel.

Although the Markov model in this paper improves on existing models, there are several potential sources of uncertainty in the model's parameters. First, all of the data used to determine the parameters were obtained from single cells rather than the averaged behavior of many cells. Therefore, any deviation of the data from the averaged behavior will be reflected in the model's parameters. Second, data from several different laboratories were used to determine the parameters and their temperature dependence. Care was taken to correct for differences in solutions and temperatures but, even so, differences in experimental technique and cell type could produce error in the parameters.

In addition to the experimental sources of uncertainty in the model's parameters, there are also sources of uncertainty in the fitting procedure. First, the parameters are sensitive to the relative weights of the cost function terms used in the minimization algorithm. By changing these weights, another set of parameters with a similar cost function value can be obtained. Therefore, the set of parameters presented here is not the only possible solution to the minimization problem. This set of parameters is, however, an acceptable solution because the amount of charge movement associated with activation and inactivation is similar to the values measured experimentally (Hodgkin and Huxley, 1952a; Oxford, 1981; Horn et al., 1984; Vandenberg and Horn, 1984; Hirschberg et al., 1995; Sheets and Hanck, 1995). It is also an acceptable set of parameters because the enthalpy, en-

tropy, and effective valence values for the $O_1 \rightarrow C_4$ and $O_1 \rightarrow I$ transitions are similar to those measured experimentally (Benndorf and Koopmann, 1993). Second, only a limited amount of experimental data can be used in the fitting process. By not including certain data in determining the model parameters, inevitably there will be data that the model does not predict. Enough data were used to constrain the model as fully as possible and to reproduce as much channel activity as possible, but not so much as to prevent timely convergence of the minimization algorithm. Moreover, as models become increasingly complex and include additional states and rate constants, inevitably there will be some parameters that are not as well constrained. The potential of unconstrained parameters was minimized by using microscopic reversibility, by assuming cooperative movement of the voltage sensors, and by requiring transitions between closed-inactivated states to have rate constants similar to those of transitions between closed states. Enough data were used to constrain the model since, as shown in Results, the model's rate constants are well determined and the model reproduces a broad range of experimental data.

There are many potential applications for the cardiac sodium channel Markov model in this paper, but there are also some limitations in the model's ability to reproduce channel activity. First, as shown in Results, the model can deviate significantly from the experimental data at the extremes of the potential range. Thus, caution should be exercised in using the model outside of the −150 mV to 20 mV range for which it was developed. Second, in order to have a model that reproduces the widest range of data possible, the best fit of a particular data set was sacrificed for good fits to all of the data sets. Applications that require the best fit of one particular data set will thus require adjustment of the model's parameters. Finally, as the temperature increases above 25°C, multiple conductance levels of the cardiac sodium channel emerge (Benndorf, 1994). The kinetics underlying these multiple conductance levels are not known, and therefore the same channel model may not apply at temperatures above 25°C. Despite these limitations, the cardiac sodium channel model reported here has many potential applications and its development is an important step in the further characterization of this channel.

APPENDIX

Calculation of the open time distributions

Figure 15 shows the simplified model from which the open time distributions are calculated. The two open states and the transitions between them are the same as for the full model shown in Fig. 1. Transitions out of each open state are lumped into a single transition from each open state to an absorbing, non-open state. It is assumed that at time zero the channel is in either O_1 or O_2. The probability of occupying each open state at time zero is equal to the transition rate from C_4 to the respective open state (γ or η) divided by the sum of these rates ($\gamma + \eta$). The probability of occupying each open state, denoted by $P_{O1}(t)$ and $P_{O2}(t)$, is then given by the solution

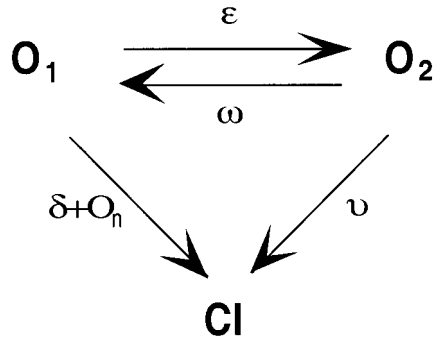

FIGURE 15 Simplified model for the computation of the open time distributions where O_1 and O_2 are the open states from the model in Fig. 1 and CI is an absorbing, non-open state. The rate constants have the same definitions as in Fig. 1.

of the following equation:

$$\frac{\partial[P_{O1}(t)\ P_{O2}(t)]}{\partial t} = \left[\frac{\gamma}{\gamma+\eta}\ \frac{\eta}{\gamma+\eta}\right] \cdot \begin{bmatrix} -\epsilon - \delta - \mathrm{On} & \epsilon \\ \omega & -\omega - \nu \end{bmatrix}. \quad \text{(A1)}$$

The solution of Eq. A1 has the form

$$[P_{O1}(t)\ P_{O2}(t)] = \left[\frac{\gamma}{\gamma+\eta}\ \frac{\eta}{\gamma+\eta}\right]\exp(\mathbf{M}t) \quad \text{(A2)}$$

where $\mathbf{M}$ is the 2×2 matrix in Eq. A1. The matrix exponential can be computed using Laplace transforms and partial fraction expansions. The resulting equations for $P_{O1}(t)$ and $P_{O2}(t)$ are as follows:

$$P_{O1}(t) = \frac{\gamma}{\gamma+\eta}[A\exp(-\lambda_1 t) + B\exp(-\lambda_2 t)] + \frac{\eta}{\gamma+\eta}[C\exp(-\lambda_1 t) + D\exp(-\lambda_2 t)] \quad \text{(A3)}$$

$$P_{O2}(t) = \frac{\gamma}{\gamma+\eta}[E\exp(-\lambda_1 t) + F\exp(-\lambda_2 t)] + \frac{\eta}{\gamma+\eta}[G\exp(-\lambda_1 t) + H\exp(-\lambda_2 t)] \quad \text{(A4)}$$

where λ_1 and λ_2 are the eigenvalues of the matrix $\mathbf{M}$ and the constants are as follows

$$A = \frac{-\lambda_1 + \omega + \nu}{\lambda_2 - \lambda_1} \quad \text{(A5)}$$

$$B = \frac{\lambda_2 - \omega - \nu}{\lambda_2 - \lambda_1} \quad \text{(A6)}$$

$$C = \frac{\omega}{\lambda_2 - \lambda_1} \quad \text{(A7)}$$

$$D = \frac{-\omega}{\lambda_2 - \lambda_1} \quad \text{(A8)}$$

$$E = \frac{\epsilon}{\lambda_2 - \lambda_1} \tag{A9}$$

$$F = \frac{-\epsilon}{\lambda_2 - \lambda_1} \tag{A10}$$

$$G = \frac{-\lambda_1 + \epsilon + \delta + \mathrm{On}}{\lambda_2 - \lambda_1} \tag{A11}$$

$$H = \frac{\lambda_2 - \epsilon - \delta - \mathrm{On}}{\lambda_2 - \lambda_1}. \tag{A12}$$

The probability of leaving the open state and entering the absorbing, non-open state is then the solution to the equation:

$$\frac{\partial CI}{\partial t} = (\delta + \mathrm{On})P_{\mathrm{O1}}(t) + \nu P_{\mathrm{O2}}(t) \tag{A13}$$

where CI is the probability of occupying the absorbing state in Fig. 15. Integrating Eq. A13 gives the distribution of the times of entering the absorbing state, which is the complement of the distribution of the open times. The distribution of the open times is given by the equation:

$$\begin{aligned} P_{\mathrm{open}}(t) = 1 &- \frac{\gamma}{\gamma + \eta}\left[\frac{(1 - \exp(-\lambda_1 t))(A\delta + A\mathrm{On} + E\nu)}{\lambda_1}\right. \\ &\left. + \frac{(1 - \exp(-\lambda_2 t))(B\delta + B\mathrm{On} + F\nu)}{\lambda_2}\right] \\ &- \frac{\eta}{\gamma + \eta}\left[\frac{(1 - \exp(-\lambda_1 t))(C\delta + C\lambda\mathrm{On} + G\nu)}{\lambda_1}\right. \\ &\left. + \frac{(1 - \exp(-\lambda_2 t))(D\delta + D\mathrm{On} + H\nu)}{\lambda_2}\right]. \end{aligned} \tag{A14}$$

The authors thank Paul Bennett, Dorothy Hanck, Michael Sheets, and Andy Wasserstrom for contributing experimental data and Paul Bennett, Dorothy Hanck, and David Yue for critically reviewing the manuscript.

This research was sponsored by National Science Foundation Grant BIR 91-17874, National Institutes of Health Grant HL60133, the Medical Scientist Training Program, the Whitaker Foundation, and Silicon Graphics, Inc.

REFERENCES

Aldrich, R. W., D. P. Corey, and C. F. Stevens. 1983. A reinterpretation of mammalian sodium channel gating based on single channel recording. *Nature.* 306:436–441.

Beeler, G. W., and H. Reuter. 1977. Reconstruction of the action potential of ventricular myocardial fibers. *J. Physiol.* 268:177–210.

Benndorf, K. 1988. Patch clamp analysis of Na^+ channel gating in mammalian myocardium: reconstruction of double pulse inactivation and voltage dependence of Na^+ currents. *Gen. Physiol. Biophys.* 7:353–378.

Benndorf, K. 1994. Properties of single cardiac sodium channels at 35°C. *J. Gen. Physiol.* 104:801–820.

Benndorf, K., and R. Koopmann. 1993. Thermodynamic entropy of two conformational transitions of single Na^+ channel molecules. *Biophys. J.* 65:1585–1589.

Berman, M. F., J. S. Camardo, R. B. Robinson, and S. A. Siegelbaum. 1989. Single sodium channels from canine ventricular myocytes: voltage dependence and relative rates of activation and inactivation. *J. Physiol.* 415:503–531.

Chay, T. R. 1991. The Hodgkin-Huxley sodium channel model versus the five-state Markovian model. *Biopolymers.* 31:1483–1502.

Clay, J. R., and L. J. DeFelice. 1983. Relationship between membrane excitability and single channel open-close kinetics. *Biophys. J.* 42: 151–157.

Colatsky, T. J. 1980. Voltage clamp measurements of sodium channel properties in rabbit cardiac Purkinje fibres. *J. Physiol.* 305:215–234.

Corana, A., M. Marchesi, C. Martini, and S. Ridella. 1987. Minimizing multimodal functions of continuous variables with the simulated annealing algorithm. *ACM Transactions on Mathematical Software.* 13: 262–280.

Correa, A. M., and F. Bezanilla. 1994. Gating of the squid sodium channel at positive potentials. II. Single channels reveal two open states. *Biophys. J.* 66:1864–1878.

Correa, A. M., F. Bezanilla, and R. Latorre. 1992. Gating kinetics of Batrachotoxin-modified Na^+ channels in the squid giant axon: voltage and temperature effects. *Biophys. J.* 61:1332–1352.

DiFrancesco, D., and D. Noble. 1985. A model of cardiac electrical activity incorporating ionic pumps and concentration changes. *Phil. Trans. R. Soc. B.* 307:353–398.

Dubois, J. M., and M. F. Schneider. 1982. Kinetics of intramembrane charge movement and sodium current in frog node of Ranvier. *J. Gen. Physiol.* 79:571–602.

Ebihara, L., and E. Johnson. 1980. Fast sodium current in cardiac muscle: a quantitative description. *Biophys. J.* 32:779–790.

Elinder, F., and P. Arhem. 1997. Tail currents in the myelinated axon of *Xenopus laevis* suggest a two-open-state Na^+ channel. *Biophys. J.* 73: 179–185.

Fozzard, H. A., and D. A. Hanck. 1996. Structure and function of voltage-dependent sodium channels: comparison of brain II and cardiac isoforms. *Physiol. Rev.* 76:887–926.

Goldman, L., and R. Hahin. 1978. Initial conditions and the kinetics of the sodium conductance in *Myxicola* giant axons. II. Relaxation experiments. *J. Gen. Physiol.* 72:879–898.

Guy, H. R. 1988. A model relating the structure of the sodium channel to its function. *Curr. Top. Membr. Transp.* 33:289–308.

Hanck, D. A., and M. F. Sheets. 1995. Modification of inactivation in cardiac sodium channels: ionic current studies with anthopleurin-A toxin. *J. Gen. Physiol.* 106:601–616.

Hanck, D. A., M. F. Sheets, and H. A. Fozzard. 1990. Gating currents associated with Na^+ channels in canine cardiac Purkinje cells. *J. Gen. Physiol.* 95:439–457.

Hille, B. 1992. Ionic Channels of Excitable Membranes. Sinauer, Sunderland, MA.

Hirschberg, B., A. Rovner, M. Lieberman, and J. Patlak. 1995. Transfer of twelve charges is needed to open skeletal muscle sodium channels. *J. Gen. Physiol.* 106:1053–1068.

Hodgkin, A. L., and A. F. Huxley. 1952a. Currents carried by sodium and potassium ions through the membrane of the giant axon of *Loligo. J. Physiol.* 116:449–472.

Hodgkin, A. L., and A. F. Huxley. 1952b. A quantitative description of membrane current and its application to conduction and excitation in nerve. *J. Physiol. (Lond.).* 117:500–544.

Hondeghem, L. M., and B. G. Katzung. 1977. Time- and voltage-dependent interactions of antiarrhythmic drugs with cardiac sodium channels. *Biochim. Biophys. Acta.* 472:373–398.

Horn, R., and C. A. Vandenberg. 1984. Statistical properties of single sodium channels. *J. Gen. Physiol.* 84:505–534.

Horn, R., C. A. Vandenberg, and K. Lange. 1984. Statistical analysis of single sodium channels: effects of n-bromoacetamide. *Biophys. J.* 45: 323–335.

Irvine, L. A., and R. L. Winslow. 1996. Numerical studies of use-dependent block of cardiac sodium channels by quinidine on spiral wave reentry. *In* Computers in Cardiology. IEEE, Indianapolis, IN. 613–616.

Jonas, P. 1989. Temperature dependence of gating current in myelinated nerve fibers. *J. Membr. Biol.* 112:277–289.

Josephson, I. R., and N. Sperelakis. 1992. Kinetic and steady-state properties of sodium channel and calcium channel charge movements in ventricular myocytes of embryonic chick heart. *J. Gen. Physiol.* 100: 195–216.

Kirsch, G. E., and A. M. Brown. 1989. Kinetic properties of single sodium channels in rat heart and rat brain. *J. Gen. Physiol.* 93:85–99.

Kohlhardt, M. 1990. Different temperature sensitivity of cardiac Na^+ channels in cell-attached and cell-free conditions. *Am. J. Physiol.* 259: C599–C604.

Kunze, D. L., A. E. Lacerda, D. L. Wilson, and A. M. Brown. 1985. Cardiac Na^+ currents and the inactivity, reopening, and waiting properties of single Na^+ channels. *J. Gen. Physiol.* 86:697–719.

Kuo, C., and B. P. Bean. 1994. Na^+ channels must deactivate to recover from inactivation. *Neuron.* 12:819–829.

Lawrence, J. H., D. T. Yue, W. C. Rose, and E. Marban. 1991. Sodium channel inactivation from resting states in guinea-pig ventricular myocytes. *J. Physiol.* 443:629–650.

Liu, S., and R. L. Rasmusson. 1997. Hodgkin-Huxley and partially coupled inactivation models yield different voltage dependence of block. *Am. J. Physiol.* 272:H2013–H2022.

Luo, C., and Y. Rudy. 1991. A model of the ventricular cardiac action potential: depolarization, repolarization, and their interaction. *Circ. Res.* 68:1501–1526.

Milburn, T., D. A. Saint, and S. Chung. 1995. The temperature dependence of conductance of the sodium channel: implications for mechanisms of ion permeation. *Receptors and Channels.* 3:201–211.

Murray, K. T., T. Anno, P. B. Bennett, and L. M. Hondeghem. 1990. Voltage clamp of the cardiac sodium current at 37°C in physiologic solutions. *Biophys. J.* 57:607–613.

Nagy, K. 1987. Evidence for multiple open states of sodium channels in neuroblastoma cells. *J. Membr. Biol.* 96:251–262.

Noda, M., T. Ikeda, T. Kayano, H. Suzuki, H. Tekeshima, M. Kuraski, H. Takahashi, and S. Numa. 1986. Existence of distinct sodium channel messenger RNAs in rat brain. *Nature (Lond.).* 320:188–192.

Noda, M., S. Shimizu, T. Tanabe, T. Takai, T. Kayano, T. Ikeda, H. Takahashi, H. Nakayama, Y. Kanaoka, N. Minamino, K. Kangawa, H. Matsuo, M. A. Raftery, T. Hirose, S. Inayama, H. Hayashida, T. Miyata, and S. Numa. 1984. Primary structure of *Electrophorus electricus* sodium channel deduced from cDNA sequence. *Nature (Lond.).* 312: 121–127.

Oxford, G. S. 1981. Some kinetic and steady-state properties of sodium channels after removal of inactivation. *J. Gen. Physiol.* 77:1–22.

Patlak, J. 1991. Molecular kinetics of voltage-dependent Na^+ channels. *Physiol. Rev.* 71:1047–1076.

Patlak, J., and M. Oritz. 1985. Slow currents through single sodium channels of the adult rat heart. *J. Gen. Physiol.* 86:89–104.

Sakakibara, Y., T. Furukawa, D. H. Singer, H. Jia, C. L. Backer, C. E. Arentzen, and J. A. Wasserstrom. 1993. Sodium current in isolated human ventricular myocytes. *Am. J. Physiol.* 34:H1301–H1309.

Scanley, B. E., D. A. Hanck, T. Chay, and H. A. Fozzard. 1990. Kinetic analysis of single sodium channels from canine cardiac Purkinje cells. *J. Gen. Physiol.* 95:411–437.

Schreibmayer, W., and G. Jeglitsch. 1992. The sodium channel activator Brevetoxin-3 uncovers a multiplicity of different open states of the cardiac sodium channel. *Biochim. Biophys. Acta.* 1104:233–242.

Sheets, M. F., and D. A. Hanck. 1995. Voltage-dependent open-state inactivation of cardiac sodium channels: gating current studies with anthopleurin-A toxin. *J. Gen. Physiol.* 106:617–640.

Sheets, M. F., J. W. Kyle, S. Krueger, and D. A. Hanck. 1996. Optimization of a mammalian expression system for the measurement of sodium channel gating currents. *Am. J. Physiol.* 271:C1001–C1006.

Starmer, C. F., A. O. Grant, and H. C. Strauss. 1984. Mechanisms of use-dependent block of sodium channels in excitable membranes by local anesthetics. *Biophys. J.* 46:15–27.

Vandenberg, C. A., and F. Bezanilla. 1991. A sodium channel gating model based on single channel, macroscopic ionic, and gating currents in squid giant axon. *Biophys. J.* 60:1511–1533.

Vandenberg, C. A., and R. Horn. 1984. Inactivation viewed through single sodium channels. *J. Gen. Physiol.* 84:535–564.

Wang, D. W., J. A. L. George, and P. B. Bennett. 1996. Comparison of heterologously expressed human cardiac and skeletal muscle sodium channels. *Biophys. J.* 70:238–245.

Yue, D. T., J. H. Lawrence, and E. Marban. 1989. Two molecular transitions influence cardiac sodium channel gating. *Science.* 244:349–351.